The Structural Properties of Uncompressed Crystalline Monolayers of Alcohols $C_nH_{2n+1}OH$ ($n = 13-31$) on Water and Their Role as Ice Nucleators

Jaroslaw Majewski, Ronit Popovitz-Biro, Wim G. Bouwman, Kristian Kjaer, Jens Als-Nielsen, Meir Lahav,* and Leslie Leiserowitz*

Abstract: A systematic analysis of grazing incidence synchrotron X-ray diffraction data of uncompressed amphiphilic alcohols $C_nH_{2n+1}OH$ ($n = 31$, 30, 23, 20, 19, 18, 16, 14, 13) on a water subphase at 5 °C is presented. Pronounced structural changes were observed on reduction of chain length from $n = 31$ to 13. The relative amount of two dimensional (2-D) crystalline material formed fell drastically; shorter crystalline coherence lengths were also observed. For $n = 31-18$ the molecules are arranged in a rectangular cell ($a \approx 5$ Å, b increases from ca. 7.4 to ca. 8.2 Å) with plane symmetry $p1g1$. For $n < 18$ a tilted free-rotator phase is probably adopted. The two glide-related molecules in the unit cell form a herringbone arrangement in which the chain axes are parallel and separated by $|(a + b)/2|$. The molecular chains are tilted from the vertical in the b direction; the tilt angle increases from ca. 7° to ca. 21° over the range $n = 31$ to 19, and then drops to 12° for $n = 13$. There is a continuous increase in molecular cross-sectional area from 18.4 to 20.3 Å^2 and in the atomic displacement parameter parallel to the water surface; it increases from 0.1 Å^2 for $n = 31$ to 0.30 Å^2 for $n = 19$. We explain the preference for chain tilt along the b axis, rather than a, in terms of hydrogen bonding to the water subphase. The various structural properties of the $C_nH_{2n+1}OH$ ($n = 31-13$) monolayer series, such as degree of crystallinity and coherence length, lattice dimensions, chain orientation, and molecular motion, may be correlated with the ice-nucleating efficiency of these alcohol monolayers as a function of n.

Keywords
alcohols · amphiphiles · GID · ice nucleators · monolayers

Introduction

In previous studies we have established that long-chain alcohols $C_nH_{2n+1}OH$ deposited in the form of monolayers on drops of water promote nucleation of hexagonal ice by virtue of a proposed epitaxy between the arrangement of ice in its *ab* plane and the two-dimensional (2-D) lattice of a monolayer.[1-4] When the water was slowly cooled, the temperature at which ice was formed was found to be dependent on chain length, that is, on the magnitude of n and on whether it was odd or even (Fig. 1).[1] Alcohols with n even (in the range 14 to 30) induced the formation of ice at a maximum temperature of −7.5 °C for $n \geq 22$; alcohols with n odd (maximum of 31) induced an asymptotic freezing temperature of −2 °C. In order to understand these results the 2-D crystal structures of the uncompressed alcohol monolayers of $C_nH_{2n+1}OH$ ($n = 20$, 23, 30, 31) on water were studied by grazing incidence X-ray diffraction (GID) with synchrotron radiation.[5-7] Here we present an analysis of the GID data of the homologous series of amphiphilic alcohols $C_nH_{2n+1}OH$ ($n = 13-31$), and correlate their structural properties with their ice-nucleating efficiency.

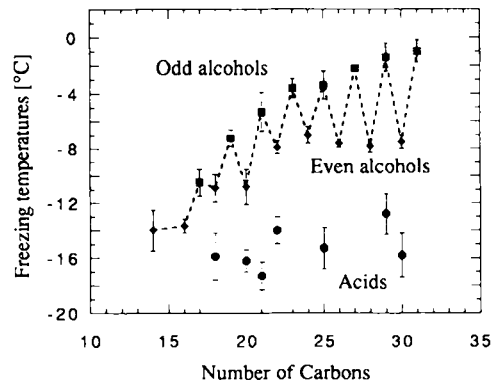

Fig. 1. Freezing temperatures of supercooled water drops covered by monolayers of amphiphilic alcohols and carboxylic acids. Temperatures are drawn separately for alcohols $C_nH_{2n+1}OH$ with n odd and even. The error bars for each point were derived from 10–20 measurements. Note the poor ice-nucleating properties of the monolayers of carboxylic acids.

Experimental Section

The GID experiments were performed at the BW1 (wiggler) beam line at the Hasylab synchrotron source (Hamburg) on a liquid surface diffractometer (Fig. 2) [9]. The synchrotron X-ray beam was monochromated to a wavelength of $\lambda = 1.37$ Å by reflection from a Be(002) in Laue geometry. The X-ray beam was adjusted to strike the surface at an incident angle of $\alpha \approx 0.85\alpha_c$, where α_c ($\approx 0.14°$ for the water subphase) is the critical angle for total external reflection. Such a geometrical configuration maximizes surface sensitivity [9, 10]. The dimensions of the footprint of the incoming X-ray beam on the liquid surface were approximately 5 × 50 mm^2. The GID patterns from the 2-D crystalline monolayers on the liquid surface arise from

[*] M. Lahav, L. Leiserowitz, J. Majewski, R. Popovitz-Biro
Department of Materials and Interfaces
The Weizmann Institute of Science
76100 Rehovot (Israel)
Telefax: Int. code + (8)34-4138
e-mail: csmajews@weizmann.weizmann.ac.il
W. G. Bouwman, K. Kjaer, J. Als-Nielsen
Department of Physics, Risø National Laboratory
DK-4000 Roskilde (Denmark)

0570-0833/95/0505-0304 $ 50.00+.25/0

a 2-D array of Bragg rods [9], which extend parallel to the vertical scattering vector q_z. In general, monolayers composed of crystallites on the water surface are azimuthally randomly oriented and so may be described as "2-D powders". Thus, the collection of the diffracted radiation by means of a position-sensitive detector (PSD), which intercepts photons over the range $0.0 \le q_z \le 0.9$ Å^{-1} ($q_z \approx 2\pi/\lambda \sin\alpha_f$, see Fig. 2) was made in two ways: The scattered intensity was measured by scanning over a range along the horizontal scattering vector q_{xy} ($\approx 4\pi \sin\theta/\lambda$, where 2θ is the angle between the incident and diffracted beam projected onto the horizontal plane)

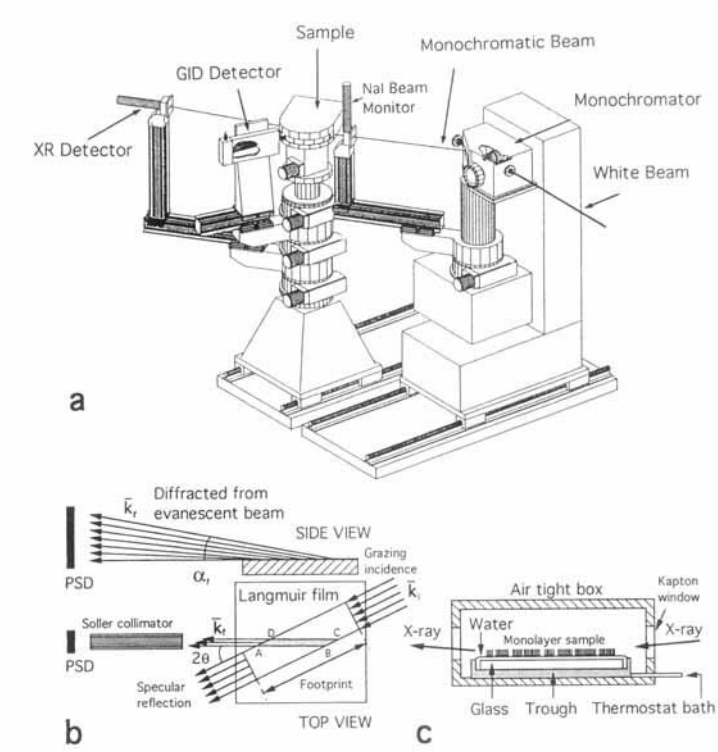

Fig. 2. a) Experimental setup of a diffractometer for studying liquid surfaces (beamline BW1, X-ray synchrotron source at Hasylab, Hamburg). The white X-ray beam is monochromated and deflected down toward the sample by tilting the Be monochromator crystal in Laue geometry. The incident and specular reflected beam intensities are monitored by the NaI Beam Monitor and the NaI XR Detector, respectively. The diffracted beam is detected with a position-sensitive detector (PSD). b) Side and top views of the grazing incidence X-ray diffraction geometry. The PSD has its axis along the vertical. Only the cross-beam area ABCD contributes to the measured scattering. The Soller collimator defines the horizontal resolution of the detector. $\boldsymbol{k}_i$ and $\boldsymbol{k}_f$ are the wave vectors of the incident and diffracted beams, respectively. The scattering vector $\boldsymbol{q}$ is given by $\boldsymbol{k}_f - \boldsymbol{k}_i$ and has vertical and horizontal components $q_z = k(\sin\alpha_f + \sin\alpha_i) \approx k \sin\alpha_f$ and $q_{xy} = k(\cos^2\alpha_f + \cos^2\alpha_i - 2\cos\alpha_f \cos\alpha_i \cos 2\theta)^{1/2} \approx 2k \sin\theta$, where $k = 2\pi/\lambda$ [13]. c) Enlarged view of the trough with monolayer spread over the thin film of water. The glass block guarantees a thin liquid film (about 0.3 mm thick) and thus effectively reduces surface capillary waves. The trough is thermostated and placed in sealed canister with Kapton windows for X-rays and mounted on the diffractometer. The canister is filled with helium gas to reduce the background of radiation scattered from air.

Abstract in Hebrew:

המבנה של צברים של כוהלים אלקניים (n = 13,14,16,18,19,20,23,31) המפוזרים על פני מים, נקבע בשיטת עקיפת קרני-x ממקור סינכרוטרון. מבנה הצברים שונה עבור אלקנים בעלי אורך שרשרת שונה. המבנה של כוהלים בעלי שרשרת באורך של n = 18 עד n = 31. המולקולות של הכוהל מסודרות בתא מלבני ($a \equiv 5$Å, ציר b גדל מ-7.4Å~ עד ל-8.2Å~), בסימטריה מישורית $p1g1$. עבור n < 18 המולקולות של הכוהל מאורגנות בפאזה של מסובב חפשי. המולקולות מתייחסות זו אל זו בתוך תא היחידה במישור החלקה תוך כדי יצירת מבנה דמוי אדרת, בהן צירי השרשרות מקבילים ומופרדים על ידי ממדים של $|(a+b)/2|$, כאשר השרשרות נטויות מן האנך בכיוון b. ההבדלים המבניים של הכוהלים על פני המים מאפשרים להסביר את ההבדלים בטמפרטורות חקפאה של טיפות מים מקוררות ביתר אשר מתלללים הכוהלים השונים.

and integrated over the whole q_z window of the PSD, to yield the *Bragg peaks*. Simultaneously, the scattered intensity recorded in channels along the PSD, but integrated over the scattering vector in the horizontal plane across a Bragg peak, produced q_z-resolved scans called *Bragg rod profiles*. For various purposes the scattered intensity data may be also presented in 2-D contour plots as a function of q_{xy} and q_z.

Several different types of information were extracted from the measured profiles. The angular position 2θ of the Bragg peaks yield the repeat distances $d = 2\pi/q_{xy}$ for the 2-D lattice structure. The Bragg peaks may be indexed by the two Miller indices h,k to yield the unit cell. The full width at half maximum (FWHM) of the Bragg peak in q_{xy} units yields the 2-D crystalline coherence length L associated with the h,k reflection, obtained by shape analysis of the Bragg peak through the Scherrer formula [11]. The intensity at a particular value of q_z in a Bragg rod is determined by the square of the molecular structure factor $|F_{hk}(q_z)|^2$. The variation of intensity I_{hk} along the Bragg rod, as a function of q_z, is given by Equation (1) (for more details see refs. [9, 12]):

$$I_{hk}(q_z) = |V|^2 |F_{hk}(q_z)|^2 \exp\{-(q_{hk}^2 u_{xy} + q_z^2 u_z)\} \quad (1)$$

The terms u_{xy} and u_z are, respectively, the mean square atomic displacements in the horizontal plane x, y, and along the vertical direction z. The factor $|V|^2$ describes the interference of X-rays diffracted upwards with rays diffracted down and subsequently reflected back up by the interface [9]. $|V|^2$ differs from unity only in the vicinity of $q_z = 0.5 q_c$ ($q_c \approx (2\pi/\lambda)\sin\alpha_c = 0.02176$ Å^{-1} for water), where it contributes a sharp peak.

Precise information on the molecular chain orientation in the 2-D crystal may be obtained from the positions of the maxima of the Bragg rods, if the aliphatic tails are uniformly and rigidly tilted in the monolayer. The tilt angle t between the molecular axis and the surface normal is given by Equation (2) [9, 13]:

$$\cos\psi_{hk} \tan t = q_z^c / |q_{hk}| \quad (2)$$

where q_z^c is the position of the maximum along the Bragg rod and ψ_{hk} is the azimuthal angle between the molecular tilt direction projected onto the xy plane and the reciprocal lattice vector $\boldsymbol{q}_{hk}$. The molecules will therefore be perpendicular to the surface when, for all reflections (h,k), q_z^c equals 0 Å^{-1}.

The measured monolayers were spread from a 5×10^{-4} M chloroform solution at about 20 °C in a thermostated Teflon trough equipped with a Wilhelmy balance for surface pressure control. The trough was placed in a sealed, helium-filled (the oxygen content was constantly monitored) canister, and the temperature was lowered to 5 °C. The monolayers were spread for 70% coverage of available water surface; this corresponds to a fully uncompressed state.

Results and Discussion

Packing Motifs of Monolayers of $C_{30}H_{61}OH$ and $C_{31}H_{63}OH$: We first review the 2-D crystal structures of $C_nH_{2n+1}OH$ (n = 30 and 31) in the uncompressed state on water at 5 °C as determined by a GID study.[6] The diffraction patterns for the two alcohols were almost identical; this indicates a similarity in their 2-D crystal structure. The molecules pack in a rectangular unit cell of dimensions listed in Table 1.

The molecular chains, which exhibit an all-trans conformation, are tilted at an angle of about 7.5° from the vertical in the direction of the b axis. The two molecules in the unit cell are related essentially by a glide plane parallel to the b axis. The molecular-chain axes lie exactly halfway between neighboring glide planes, so that we may, to a first approximation, regard the unit cell as c-centered, that is, the long molecular axes are positioned at x, y, z and $\frac{1}{2} + x$, $\frac{1}{2} + y$, z. The molecular chains are oriented with respect to the glide plane such that the dihedral angle between glide-related hydrocarbon planes is approximately 90°.

There is an ambiguity in fixing the azimuthal orientation of the molecule, which may adopt either of the two structures shown in Figure 3 for say n = 31. Since the hydrocarbon chain has a regular zig-zag arrangement with local mg symmetry, the two orientations are essentially equivalent but for the OH and CH_3 groups. However, the two orientations do not in general yield the same intermolecular contacts. The odd–even effect for n = 30 and 31 in the ice-nucleation experiments,[1] complemented by the GID results, indicates that the hydrocarbon chain structure is the same for both n = 30 and

Table 1. Structural data of the uncompressed (70% surface coverage) alcohol monolayer series $C_nH_{2n+1}OH$ (n = 31–13) at 5 °C on pure water.

n	a/Å	b/Å	b proj./Å [a]	A_x/Å^2 [b]	A_x proj./Å^2 [c]	t/° [d]	δ/° [e]	a_H/Å [f]	γ_H/° [f]	η/° [g]	η'/° [h]
31	4.98	7.45	7.39	18.6	18.4	7.0 [i]	1.5	4.46	112.1	90	90
30	4.99	7.49	7.42	18.7	18.5	7.7	1.7	4.47	112.1	86	90
23	5.00	7.56	7.46	18.9	18.6	9.5	1.2	4.49	112.3	82	110
20	5.05	8.00	7.56	20.2	19.1	19.0	2.4	4.55	112.6	130	130
19	5.03	8.13	7.60	20.4	19.1	20.8	2.0	4.56	113.1	130	130
18	4.99	8.19	7.73	20.4	19.2	19.4	2.9	4.60	114.5	120	130
17	4.94	8.34	7.91	20.6	19.5	18.5	2.5	4.66	116.0	130	130
16	4.86	8.41	8.09	20.4	19.6	15.8 [j]	2.8 [j]	4.72	118.2	120	130
14	4.84	8.47	8.19	20.5	19.8	14.8 [j]	3.0 [j]	4.75	118.9	120	130
13	4.86	8.55	8.36	20.8	20.3	12.0	3.0	4.83	119.7	130	130

[a] b axis projected: $b\cos t$ (a axis projected: $a\cos\delta \approx a$). [b] Area per molecule = $ab/2$. [c] Projected area per molecule = $ab\cos t/2$. [d] Tilt angle measured from the normal to the water surface in the direction of the b axis. [e] Tilt angle measured from the normal to the water surface in the direction of the a axis. [f] Pseudo-hexagonal representation of the rectangular cell projected along the molecular axis. [g] Obtained from the Bragg rod fits. The dihedral angle between the molecular planes of two molecules related by pseudo-glide symmetry subtended along the a axis. [h] Obtained from lattice energy calculations. The dihedral angle between the molecular planes of two molecules related by glide symmetry subtended along the a axis. [i] Average tilt. [j] Observed Bragg rod fitted with {1,1} and {0,2} simultaneously.

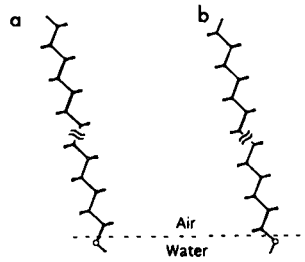

Fig. 3. Schematic view of the two possible orientations, a and b, of amphiphilic alcohol $C_{31}H_{63}OH$ on the horizontal water surface in the 2-D crystal.

31 and that the orientations of their C–OH groups with respect to water are different; however, the orientation adopted by the hydrocarbon chain, and consequently that of the C–OH group, remains uncertain.

2-D Crystal Structure Determination of $C_nH_{2n+1}OH$ (n = 13–31): In general, the GID data of the monolayers $C_nH_{2n+1}OH$ (n = 13–31) yields two low-order reflections, which are indexed as {1,1} and {0,2} describing a rectangular cell. As n decreases from 31, the resolved {1,1} and {0,2} reflections tend to converge until n = 16, at which point they coincide, and the corresponding $d_{\{1,1\}}$ and $d_{\{0,2\}}$ spacings are thus equal (see Fig. 4b).

Below n = 16 the trend continues, and the Bragg positions of the two reflections cross over and once again tend to be resolved, as is evident for n = 14 and 13 from the two-dimensional intensity plots $I(q_{xy}, q_z)$ and Bragg peak profiles $I(q_{xy})$ shown in Figs. 4 and 5, respectively. The 2-D packing arrangements in the

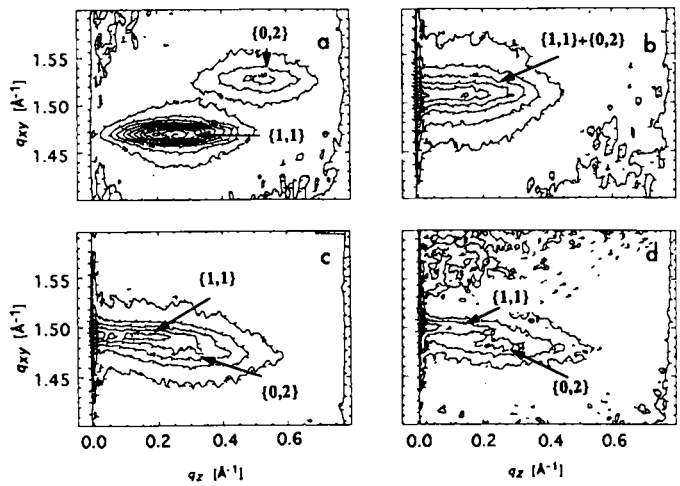

Fig. 4. Grazing incidence X-ray diffraction measurements from four uncompressed monolayers of a) $C_{18}H_{37}OH$, b) $C_{16}H_{33}OH$, c) $C_{14}H_{29}OH$, and d) $C_{13}H_{27}OH$ at 5 °C on the water surface. The 2-D contour plots of the intensity distribution $I(q_{xy}, q_z)$ along the horizontal (q_{xy}) and the vertical (q_z) scattering vectors are shown. The positions of intensity maxima of the {1,1} and the {0,2} reflections are not the same for the four alcohols; this indicates different unit cell dimensions and angles of molecular tilt.

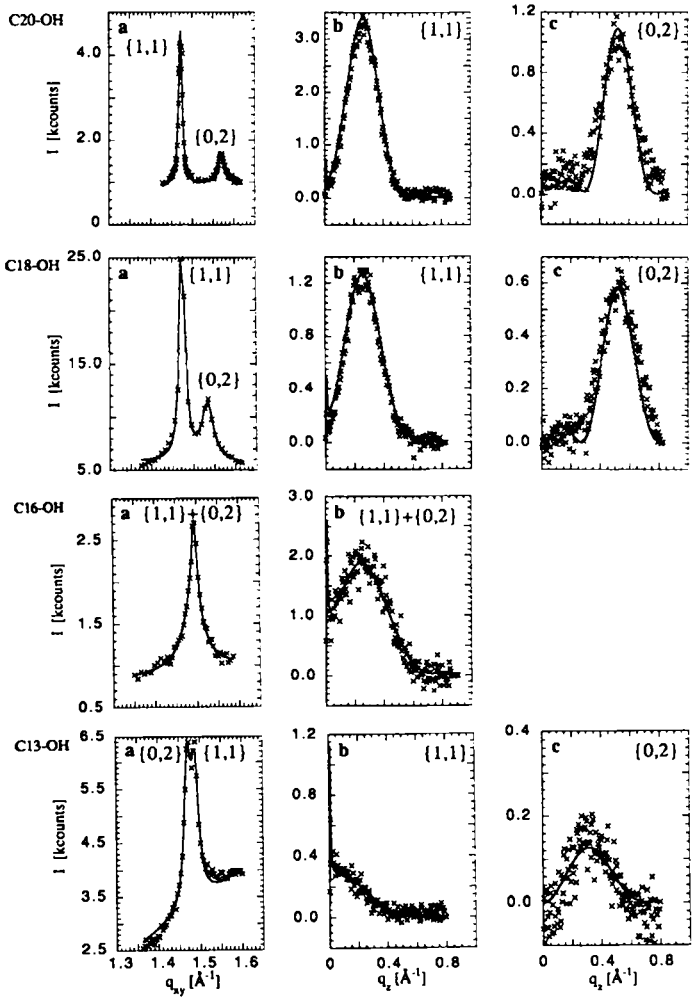

Fig. 5. Measured (x) and calculated (—) grazing incidence X-ray diffraction data for $C_{20}H_{41}OH$, $C_{18}H_{37}OH$, $C_{16}H_{33}OH$, and $C_{13}H_{27}OH$: a) Bragg peak profiles obtained by scanning along the horizontal scattering vector q_{xy} ($\approx(4\pi\sin\theta)/\lambda$, where 2θ is the horizontal angle between the incident and diffracted beam) and integrating over the whole q_z window of the PSD. b) and c) Scattered intensity distribution perpendicular to the water surface and integrated over q_{xy} range of each Bragg peak to yield Bragg rods. These rods were fitted by molecular structure-factor calculations (see Experimental Section). The molecular packing parameters used in the fitting procedure are listed in Table 1.

0570-0833/95/0505-0306 $ 50.00+.25/0

$C_nH_{2n+1}OH$ series were determined by fitting a molecular model to the observed Bragg rod data with Equation (1). This analysis yielded good fits to the Bragg rod profiles for all monolayers (Fig. 5).

The 2-D crystal structures for $n = 16$ and 14 were determined by using the unresolved, or barely resolved, {1,1} and {0,2} Bragg rods. The feasibility of such a refinement procedure was tested by fitting the molecular structure of $C_{18}H_{37}OH$ to a composite Bragg rod of the resolved {1,1} and {0,2} reflections added together; this yielded a structure almost identical to that obtained with resolved peaks. For $n = 13$ we were able to resolve and then fit the {1,1} and the {0,2} Bragg rods separately. Some structural results are given in Table 1. In the refinement of each crystal structure we assumed the plane group symmetry $p1g1$ (i.e., a primitive cell containing two molecules related by a glide plane perpendicular to the a axis). In order to improve the fit to the observed Bragg rod profiles the plane group symmetry was relaxed by allowing the glide plane to lean from the vertical plane by an angle δ about a horizontal axis parallel to b (Fig. 6).

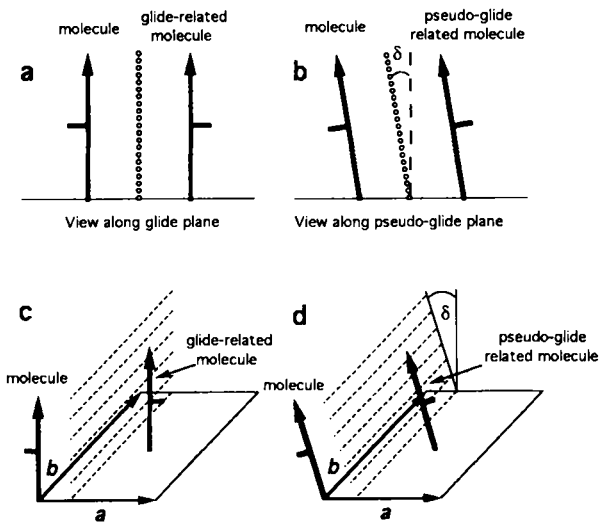

Fig. 6. a) and c) Schematic representation of glide-related molecules in $p1g1$ plane symmetry. The glide plane is parallel to the b axis. b) and d) Schematic view of relaxed $p1g1$ symmetry. Here the glide plane is tilted in the direction of the a axis by a small angle δ, and the molecules are no longer related by pure crystallographic symmetry, although an angle of 90° between the a and b axes is still preserved. Such an arrangement was found to improve the fit between the calculated and observed Bragg rod intensity profiles.

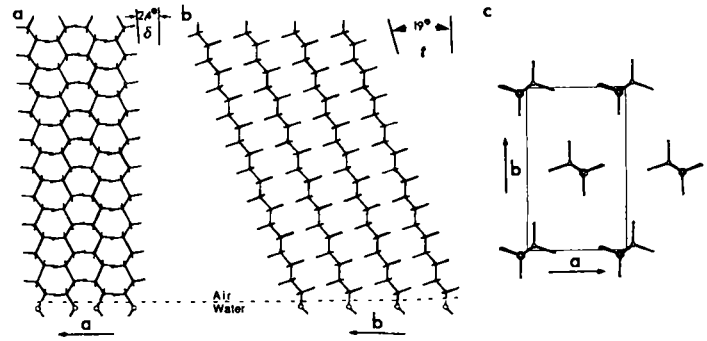

Fig. 7. Molecular packing arrangement for $C_{20}H_{41}OH$ in the 2-D crystal. All molecules are tilted by $t = 19°$ from the vertical in the direction of the b axis and by $\delta = 2.4°$ in the direction of the a axis: a) view along the b axis; b) view along the a axis; and c) view along the molecular axis. Because of the ambiguity in fixing the absolute azimuthal orientation of the hydrocarbon chain, we have arbitrarily chosen one of the two possible orientations.

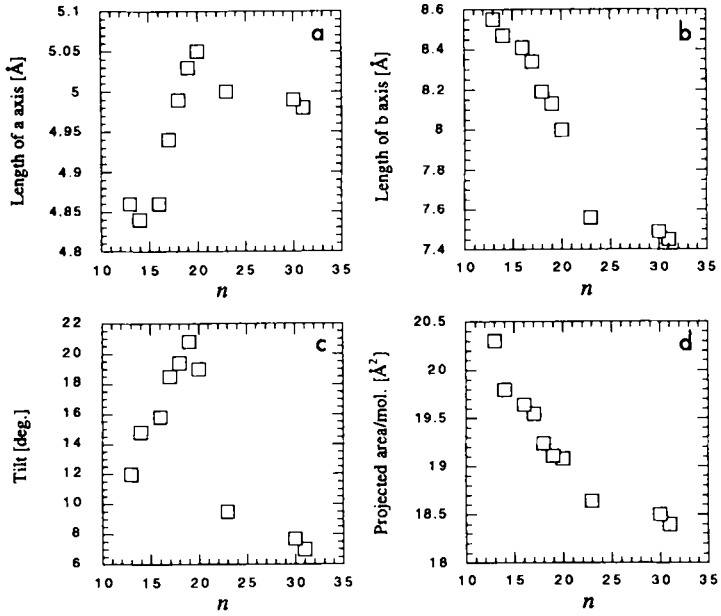

Fig. 8. Various molecular packing properties of the amphiphilic $C_nH_{2n+1}OH$ 2-D crystal structures as a function of n.

Refinement of the Bragg rod data yielded δ values ranging from 1.5° for $n = 31$ to 3° for $n = 13$ (Table 1). The resulting plane symmetry group is thus no longer $p1g1$, but $p1$ with two independent molecules per unit cell. Such a "pseudo-glide" packing arrangement yields only a minor distortion from the pure glide motif and still preserves the herringbone motif of the hydrocarbon chains,[14] as shown for $C_{20}H_{41}OH$ in Figure 7.

Comparison of the 2-D Crystalline Properties of the $C_nH_{2n+1}OH$ Series: The change in crystal structure as a function of chain length, in terms of cell dimensions, molecular tilt, and cross-sectional area per molecule, is depicted in Figure 8. The a axis shows only a minor decrease in length, by about 0.15 Å from $n = 18$ to 13 (Fig. 8a). There is a slight increase in the length of the b axis from $n = 31$ to 23 followed by a steeper increase till $n = 13$ (Fig. 8b). The molecular tilt angle t follows an irregular profile (Fig. 8c). Starting with 7° for $n = 31$, there is a minor increase of 2° for $n = 23$, followed by a jump of about 10° for $n = 20$, 19, and 18. Surprisingly, the chain tilt decreases to 12° at the lower limit $n = 13$, despite a continuous increase in the length of the b axis. The cross-sectional molecular area A_x ($= A\cos t$, where A is the surface molecular area $ab/2$) rises continuously from 18.4 to 20.3 Å^2 across the whole range of n (Fig. 8d).[15] This increase extends only in the b direction. We interpret this result in terms of a continuous increase in molecular motion parallel to the water surface with decreasing chain length.[16]

As mentioned previously, the full width at half maximum of the Bragg peak, corrected for the resolution of the spectrometer, yields the 2-D crystalline coherence length L associated with the hk crystallographic direction. The coherence lengths are anisotropic, particularly for the longer chains, and become smaller with decreasing chain length (Fig. 9).[17] The crystalline coherence lengths for $C_{31}H_{63}OH$ were found to be anisotropic with values of ca. 1000 Å and ca. 300 Å along the {1,1} and {0,2} crystallographic directions, becoming almost isotropic and as small as 300 Å for $C_{13}H_{27}OH$.

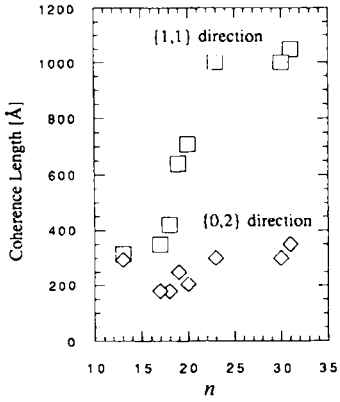

Fig. 9. Crystal coherence lengths (L) deduced from the {1,1} and {0,2} reflections, obtained by width analysis of the Bragg peaks with the Scherrer formula. L from the {2,0} reflection (observed for $n = 23$, 30 and 31) was resolution-limited and is thus > 1000 Å. For $n = 16$ and 14 the two {1,1} and {0,2} reflections were unresolved. The analysis of the resolved {1,1} and {0,2} reflections for $n = 13$ gave almost identical coherence lengths along both crystallographic directions.

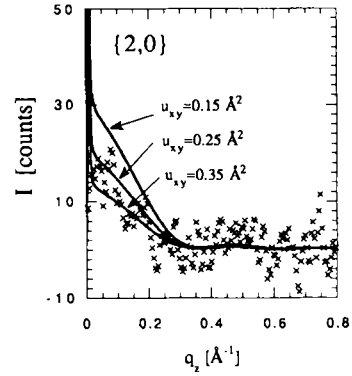

Fig. 10. The observed Bragg rod intensity profile of the {2,0} reflection of the $C_{19}H_{39}OH$ monolayer (x) and the calculated profiles (—) as a function of in-plane atomic displacement parameter u_{xy}. The influence of u_{xy} on the calculated {1,1} and {0,2} Bragg rod profiles (not shown here) was minor. The temperature parameter u_z along the vertical axis was set at 0.5 Å². To decrease the statistical scatter of the observed data along q_z, we averaged every three data points. Note that the net integrated intensity along q_z for the observed Bragg rod is 2.77 and those for the calculated rods for u_{xy} = 0.15, 0.25, and 0.35 Å² are 5.46, 3.66, and 2.46, respectively, in arbitrary units.

We have been able to extract the relative amount of 2-D crystalline material from a comparison of the factor that scales the measured and calculated Bragg rod intensities[9] of the monolayers $C_nH_{2n+1}OH$ (n = 31, 20, 16) under constant experimental conditions. The relative amounts of crystalline material are 1:0.33:0.25 for n = 31, 20, and 16, respectively.

Molecular Motion in the $C_nH_{2n+1}OH$ Series: The increase in molecular cross-sectional area A_x with decreasing chain length (Fig. 8d) may be associated with an increase in molecular motion. Evidence for this correlation is provided by the fact that the cross-sectional area of alcohols and diols with long hydrocarbon chains decreases when the temperature is lowered. For example, according to GID data reported by Shih et al.,[19] the molecular cross-sectional area of a crystalline monolayer of $C_{21}H_{43}OH$ in the uncompressed state on a water surface increases from 19.8 to 20.4 Å² with a temperature rise from 22 to 33 °C. In the 3-D crystalline state, the molecular cross-sectional area of $C_{24}H_{49}OH$ at −175 °C is as low as 17.4 Å²;[20] by comparison, the 3-D crystal structure of $C_{16}H_{33}OH$ at room temperature has a molecular cross-sectional area of 18.7 Å².[21] This result is in agreement with that for the 3-D crystal structure of $HOC_9H_{18}OH$, whose cross-sectional area at low temperature (−175 °C) is 1.0 Å² less than at room temperature.[6]

A direct estimate of the average atomic displacement (or Debye–Waller) parameter[22] parallel to the water surface, u_{xy}, can be derived from the GID data for the longer chain alcohols (n = 31, 30, 23, 20, and 19).[23] This value was estimated by varying u_{xy} to best fit the Bragg rod profiles, particularly for the higher order reflections. A value of around 0.1 Å² was computed for n = 31, 30, and 23 by making use of the {1,1}, {0,2}, and {2,0} reflections.[6] The presence, albeit weak, of the higher order {2,0} reflection for $n = 20$ and 19 yielded values of u_{xy} = 0.13 and 0.30 Å², respectively (Fig. 10). Below $n = 19$ the {2,0} reflection was not observed; this allowed us to deduce, by structure-factor calculations, that $u_{xy} \geq 0.35$ Å².

To estimate the atomic displacement parameter for the lower limit of n, we calculated the average H···H contacts in the 2-D crystal structures of the $C_nH_{2n+1}OH$ series (Fig. 11). We obtained a *rough* estimate of u_{xy} for $n = 19$ vs. that for n = 31 by assuming that the molecules of $C_{19}H_{39}OH$ undergo sufficient additional motion for neighboring H atoms to come into contact. The average increase in nearest-neighbor H···H distances on going from n = 31 to 19 is approximately 0.3 Å. Thus, given the atomic displacement $u_{xy}^{1/2}$ of around 0.3 Å for the carbon atoms of $C_{31}H_{63}OH$, the value for $n = 19$ would be around 0.45 Å (0.3 + 0.3/2 Å); this value yields a molecular displacement parameter $u_{xy} \approx 0.2$ Å², which is close to the value of 0.3 Å² obtained from GID.

Testing the Free-Rotator Phase: For all the monolayer systems we have assumed a herringbone structure. It had been proven previously,[6] by an analysis of the GID results, complemented by lattice energy calculations, that the monolayers of $C_nH_{2n+1}OH$ (n = 31, 30, 23) do indeed exhibit a herringbone arrangement with a fixed azimuthal orientation of the hydrocarbon chains. Assuming that the a,b unit cell is c-centered, the dimensions of such a cell projected along the molecular axis a_p, b_p ($a_p = a\cos\delta \approx a$, $b_p = b\cos t$), expressed in terms of the pseudo-hexagonal representation ($a_H = b_H = 0.5(a_p^2 + b_p^2)^{1/2}$, $\gamma_H = 2\arccos(0.5a_p/a_H)$), are given in Table 1. We observe from Table 1 that γ_H tends to an angle of 120° as n approaches 13; this is indicative of a hexagonal cell in projection. The projected molecular area A_x reaches a value of 20.3 Å² for $n = 13$, which is very close to that corresponding to a presumably free-rotator phase in the alcohol $C_{21}H_{43}OH$ at 33 °C in the uncompressed state[19] and the rotator I–II phases of $C_{20}H_{41}COOH$ in the compressed state.[24] We therefore tested, by structure-factor calculations, the effect of a *tilted* free-rotator phase on the Bragg rod intensity profiles for $n = 13$. For practical purposes we constructed a model composed of 12 azimuthal orientations of the chain, each with a molecular occupancy of $^1/_{12}$, covering a full circle of 360°. The fit of such a model (Fig. 12) to the scattering data is no worse than for the herringbone arrangement (Fig. 5). A similar analytical procedure was carried out for $n = 18$, which had a projected cross-sectional area $A_x = 19.4$ Å² and $\gamma_H = 114.5°$. A model that simulated the free rotator yielded a poor fit to the Bragg rod data, particularly for the {0,2} reflection. Indeed, assuming pronounced librational motion about the molecular axis corresponding to a libration angle greater than ±20° from the mean azimuthal angle in the herringbone arrangement also gave a poor fit to the {0,2} reflection (Fig. 13).

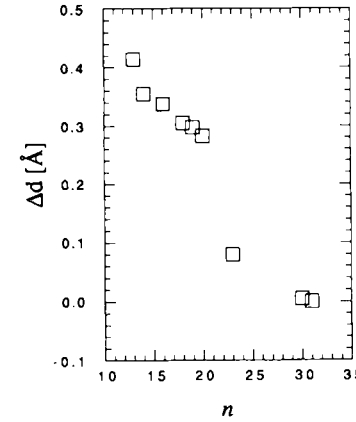

Fig. 11. The change in average H···H intermolecular contact distance Δd in the 2-D crystal structures of $C_nH_{2n+1}OH$ (n = 31–13) as determined by GID. The average H···H distance for n = 31 is 2.7 Å.

We also calculated the variation in lattice energy as a function of rotation of the molecule about its chain axis, while maintaining the herringbone structure in accordance with the glide sym-

0570-0833/95/0505-0308 $ 50.00+.25/0 Chem. Eur. J. 1995, 1, No. 5

metry. In the two extreme cases $n = 31$ and $n = 13$, the variation is much shallower for the latter system (Fig. 14), in keeping with the greater tendency towards free rotation as the chain is shortened.

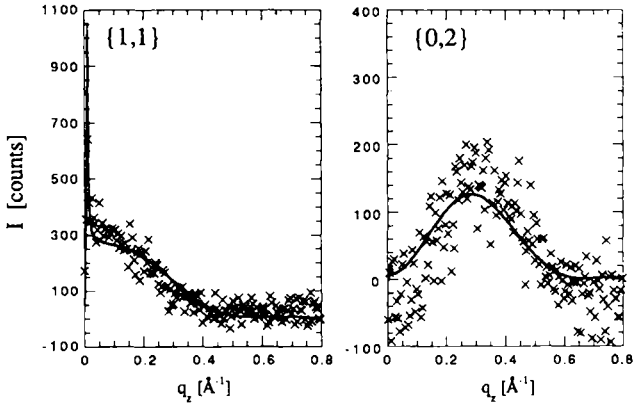

Fig. 12. Measured (x) and calculated (—) grazing incidence X-ray diffraction data for $C_{13}H_{27}OH$. The Bragg rod intensity profiles were fitted by using molecular structure-factor calculations assuming a tilted free-rotator model. The composite molecule used in the calculations was composed of 12 azimuthal orientations covering the full 360°, each with a molecular occupancy of $^1/_{12}$. The tilt and lean angles obtained by least-square refinement were: $t = 11.9°$ and $\delta = 2.8°$.

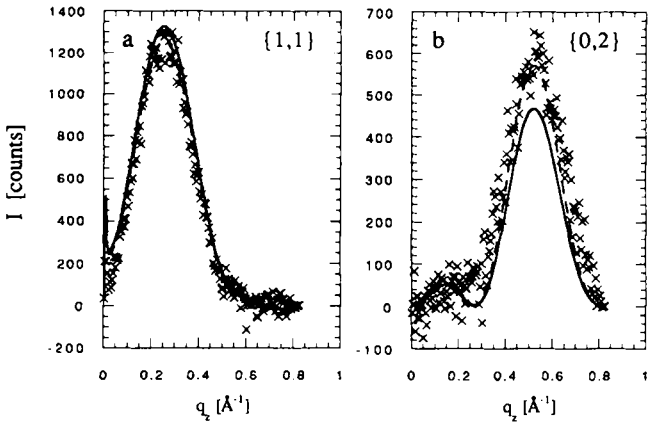

Fig. 13. Measured (x) and calculated grazing incidence X-ray diffraction data for $C_{18}H_{37}OH$. The Bragg rod intensity profiles were fitted by using molecular X-ray structure-factor calculations assuming a tilted free-rotator model (—) as against a herringbone arrangement of molecular chains (- - -).

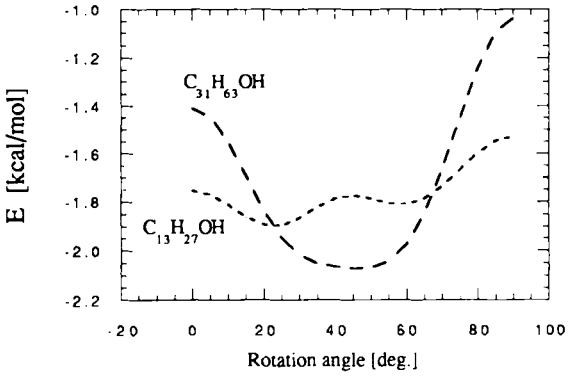

Fig. 14. The calculated variation in lattice energy E per CH_2 group (kcal mol^{-1}) as a function of the rotation of $C_nH_{2n+1}OH$ about its chain axis for the two extremes $n = 13$ and 31.

Effect of Water Subphase on Molecular Packing: The question arises as to why the continuous rise in cross-sectional molecular area over the range $n = 31$ to 13 requires a concomitant increase in tilt angle along the b axis from $n = 31$ to 19 and then a fall in tilt angle from $n = 19$ to 13. At first sight, it might seem that an increased tilt angle leads to a lower stabilization energy in the 2-D crystal structures, because of possible end-of-chain effect and relative offsetting between neighboring chains. The rise in calculated monolayer lattice energy per CH_2 group for $C_nH_{2n+1}OH$[14] is minor (Fig. 15) for an increase in molecular tilt angle from 7 to 21° and a concomitant increase of the b axis from 7.45 to 8.13 Å (i.e., $n = 31$ to 19). Only as the tilt angle gradually decreases from 21 to 12° for $n = 19$ to 13, with a continuous increase in length of the b axis to 8.55 Å and in molecular cross-sectional area, is there a substantial increase in calculated lattice energy (Fig. 15). Clearly the calculated lattice energy cannot be correct for $n < 18$, in view of the fact that these structures tend to be free rotators. Nevertheless, the calculated lattice energy must increase with increasing cross-sectional area for $n < 18$, in accordance with the shape of the van der Waals potential, although we cannot be sure that the given energies can be regarded as threshold values.

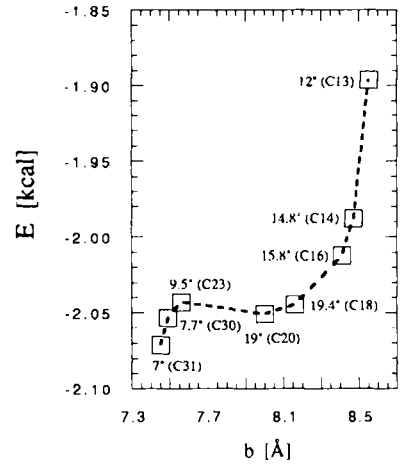

Fig. 15. Calculated lattice energy E per CH_2 group (kcal mol^{-1}) for the alcohol series $C_nH_{2n+1}OH$ ($n = 13$, 14, 16, 18, 20, 23, 30, and 31). The calculations were performed by using glide-related molecules and structural parameters (a, b, and tilt angle) obtained from the grazing incidence X-ray diffraction experiments. The energy minimum for each alcohol was found by allowing the molecule to rotate around its long axis. The van der Waals parameters, atomic net charge, dipole and quadrupole moments were taken from ref. [14]. The energies calculated for $n < 18$ must be regarded as a threshold values, since they were obtained assuming the herringbone arrangement and not a free-rotator phase. Note that the binding energy to the water subphase was ignored.

We can at least explain the preference for tilt along the b axis rather than the a axis in terms of hydrogen bonding to the subphase water molecules. Our basic premise is that a water molecule will form acceptable hydrogen bonds with two neighboring alcohol molecules provided the distance between the two lies in the range of 4.5–5.0 Å, based on the 3-D crystal structures of ice, methanol, and other alcohols.[25] Thus, a tilt along the a axis could be detrimental to hydrogen bonding since the length of the a axis with the molecular chains vertically aligned is 5 Å, the maximum threshold distance. On the other hand, an increase in molecular tilt from 7 to 21° along the b axis results in an increase in axial length from ca. 7.4 to ca. 8.1 Å, which is satisfactory for hydrogen bonding since the distance between glide-related molecules along the diagonal $\frac{1}{2}|a + b|$ would then increase from 4.5 to 4.8 Å. Indeed, in the 3-D crystal structures

of the long-chain alcohols $C_nH_{2n+1}OH$ ($n = 16, 24$),[21, 6] molecules are highly tilted in the direction of the b axis; this leads to good hydrogen bonding between molecular layers.

The decrease in tilt angle from 21° for $C_{19}H_{39}OH$ to 12° for $C_{13}H_{27}OH$ and the concomitant increase in molecular cross-sectional area can be rationalized in terms of hydrogen bonding. Had the molecular chains retained the tilt angle of 21° with the observed increase in cross-sectional area A_x, the b axis would have increased from ca. 8.1 to ca. 8.9 Å; this would result in a separation between glide-related chains of 5.1 Å, which is longer than the threshold distance for hydrogen bonding.

Monolayer Packing of $C_nH_{2n+1}OH$ and Their Ice-Nucleating Behavior: The various changes in the 2-D crystalline properties of the alcohol series can be correlated with their ice-nucleating behavior (Fig. 1). The significant decrease in the amount of 2-D crystalline material formed and in crystalline coherence length as a function of decreasing chain length in the range $n = 31$ to 13 (see Fig. 9) is certainly consistent with the ice-nucleating curve. A more quantitative description can be provided for the role of the lattice match with that of ice. The *ab* lattices of $C_{31}H_{63}OH$ and of hexagonal ice are depicted in Figure 16a and b, respectively. The superposition of the *ab* nets of $C_{31}H_{63}OH$ and of $C_{13}H_{27}OH$ onto the *ab* lattice of hexagonal ice are shown in Figure 17. The mean value of the distances between closest lattice points over a local cluster of around 40 Å in diameter is 0.9 Å for $C_{31}H_{63}OH$ and 1.1 Å for $C_{13}H_{27}OH$; this indicates that the lattice match is better for $C_{31}H_{63}OH$. This result is also consistent with the fact that the molecular area *ab*/2 of the alcohol chains $C_nH_{2n+1}OH$ increases from 18.6 to 20.8 Å^2 when n is decreased from 31 to 13; the *ab* layer area of hexagonal ice is 17.5 Å^2. The odd–even effect in ice-nucleating behavior is clearly due to a difference in C–OH orientation with respect to the water surface. However, we are not able to fix the absolute orientation of the hydrocarbon chains and so resolve the ambiguity in C–OH orientations in the odd and even alcohol $C_nH_{2n+1}OH$ series. A problem of this type was solved in the series $C_nH_{2n+1}CO_2C_mH_{2m}OH$ (m odd and even) by unambiguous determination of the structures of the two monolayers with $n = 19$ and $m = 9$, 10. According to the GID data, complemented by lattice energy calculations[6] and the ice-nucleation experiments, the chain structure was found to be essentially identical in the two monolayers, but the orientations of the C–OH groups with respect to the water differed.

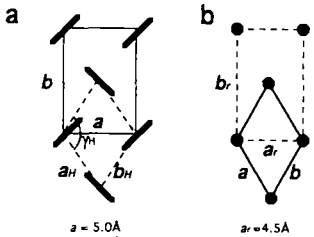

Fig. 16. a) Schematic view of the orthogonal packing of hydrocarbon chains of the $C_{31}H_{63}OH$ monolayer in a rectangular unit cell (a,b; $a = 5.0$, $b = 7.4$ Å), viewed along the chain axis. The distorted hexagonal representation of the cell is also depicted (a_H,b_H). b) Schematic view of the unit cell of hexagonal ice (viewed along the c axis) in terms of the hexagonal cell (a,b) and a c-centered rectangular cell (a_r,b_r; $a_r = 4.5$, $b_r = 7.8$ Å). Note the match between the unit cell of the alcohol monolayer and that of ice.

Finally, we consider the effect of molecular motion on ice-nucleating behavior. The significant increase in molecular motion with decrease in chain length in the $C_nH_{2n+1}OH$ series implies a concomitant weakening of hydrogen bonds between the C–OH groups of an alcohol monolayer and the ice layer that is in the process of being formed. This model is consistent with the observed change in ice-nucleating efficiency as a function of chain length. The role of molecular motion also allows us to rationalize the better ice-nucleating properties of $C_{19}H_{39}CO_2C_mH_{2m}OH$ ($m = 9$, 10) compared to $C_nH_{2n+1}OH$ ($n = 18$, 19): in both types of monolayers, the molecules are highly tilted (by 25 and 21°, respectively) from the normal to the water. For the carboxy ester alcohols the molecular displacement parameter u_{xy} was found by GID to be around 0.1 Å^2, corresponding to an amplitude of motion of about 0.3 Å. The amplitude of motion for the alcohols $C_{19}H_{39}OH$ and $C_{18}H_{37}OH$ was estimated to be as high as $0.3^{1/2} \approx 0.6$ Å.

Conclusions

Various structural properties of uncompressed crystalline monolayers of $C_nH_{2n+1}OH$ ($n = 13$–31) on water at 5 °C were determined by grazing incidence X-ray diffraction. These properties include relative amount of crystalline material formed, crystalline coherence length, molecular packing arrangements, and molecular motion. Furthermore, we correlated these structural characteristics of the alcohol monolayers with their ice-nucleating behavior as a function of chain length. The interplay between the molecular packing of the alcohol monolayers and the water or ice subphases still remains to be properly understood and experimentally characterized, although molecular simulations[26, 27] and nonlinear optical measurements[28] have been performed on some model systems. Some light may be shed on this problem by changing the subphase to formamide, which is known to support amphiphilic crystalline monolayers.[29]

Acknowledgement: We acknowledge financial support from the Minerva Foundation and the Danish Foundation for Natural Sciences.

Received: November 25, 1994 [F23]

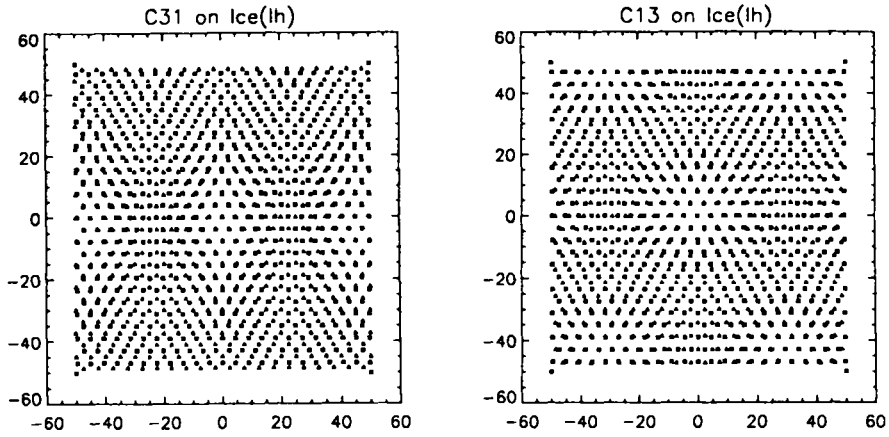

Fig. 17. A diagram of the oxygen positions within the *ab* layer of hexagonal ice (triangles) superimposed on the oxygen positions in monolayers (squares) of $C_{31}H_{63}OH$ (left) and $C_{13}H_{27}OH$ (right).

0570-0833/95/0505-0310 $ 50.00+.25/0

[1] M. Gavish, R. Popovitz-Biro, M. Lahav, L. Leiserowitz, *Science* **1990**, *250*, 973.
[2] R. Popovitz-Biro, J. L. Wang, J. Majewski, E. Shavit, L. Leiserowitz, M. Lahav, *J. Am. Chem. Soc.* **1994**, *116*, 1179.
[3] J. Majewski, L. Margulis, D. Jacquemain, F. Leveiller, C. Böhm, T. Arad, Y. Talmon, M. Lahav, L. Leiserowitz, *Science* **1993**, *261*, 899.
[4] J. Majewski, R. Popovitz-Biro, K. Kjaer, J. Als-Nielsen, M. Lahav, L. Leiserowitz, *J. Phys. Chem.* **1994**, *98*, 4087.
[5] D. Jacquemain, F. Leveiller, S. P. Weinbach, M. Lahav, L. Leiserowitz, K. Kjaer, J. Als-Nielsen, *J. Am. Chem. Soc.* **1991**, *113*, 7684.
[6] J. L. Wang, F. Leveiller, D. Jacquemain, K. Kjaer, J. Als-Nielsen, M. Lahav, L. Leiserowitz, *J. Am. Chem. Soc.* **1993**, *116*, 1192.
[7] The studies given in refs. [5] and [6] were preceded by a GID study of $C_{21}H_{43}OH$ monolayer on water at 0–10 °C, but in the compressed state [8].
[8] T. M. Bohanon, B. Lin, M. C. Shih, G. E. Ice, P. Dutta, *Phys. Rev. B*, **1990**, *41*, 4846.
[9] J. Als-Nielsen, K. Kjaer in *Proceedings of the NATO Advanced Study Institute, Phase Transitions in Soft Condensed Matter* (Eds.: T. Riste and D. Sherrington), Plenum Press, New York, Geilo, Norway, **1989**, p. 113.
[10] R. Feidenhans'l, *Surf. Sci. Rep.* **1989**, *10* (3), 105.
[11] A. Guinier, *X-ray Diffraction*, Freeman, San Francisco, **1968**.
[12] D. Jacquemain, F. Leveiller, S. Grayer-Wolf, M. Deutsch, K. Kjaer, J. Als-Nielsen, M. Lahav, L. Leiserowitz, *Angew. Chem. Int. Ed. Engl.* **1992**, *31*, 130.
[13] K. Kjaer, *Proceedings of the 3rd Int. Conference on Surface X-ray and Neutron Scattering, Dubna, Russia, 1993*, *Physica B*, **1994**, *100*.
[14] F. Leveiller, D. Jacquemain, K. Kjaer, J. Als-Nielsen, L. Leiserowitz, *J. Phys. Chem.* **1992**, *96*, 10380.
[15] J. F. Legrand, A. Renault, O. Konovalov, E. Chevigny, J. Als-Nielsen, G. Grübel, B. Berge, *Thin Solid Films* **1994**, *248*, 95. It is noteworthy that a monolayer of $C_{14}H_{29}OH$ on water at 2 °C in a highly compressed state (40–50 $mN\,m^{-1}$) crystallizes in a hexagonal arrangement, owing to the fact that an excess drop on the water serves as a reservoir. The molecules are vertically aligned with a cross-sectional area per molecule of 20.4 $Å^2$; this is close to the value that we obtained in an uncompressed tilted state.
[16] This motion is related to the tilted free-rotater phase model described below.
[17] Reductions in the amount of crystalline material as a function of chain length and in the anisotropic crystalline coherence length as a function of molecular tilt have been examined in terms of lattice energy calculation [14,18].
[18] D. Jacquemain, S. Grayer-Wolf, F. Leveiller, F. Frolow, M. Eisenstein, M. Lahav, L. Leiserowitz, *J. Am. Chem. Soc.* **1992**, *114*, 9983.
[19] M. C. Shih, T. M. Bohanon, J. M. Mikrut, P. Zschack, P. Dutta, *J. Chem. Phys.* **1992**, *97*, 4485.
[20] J. L. Wang, Ph.D. Thesis, The Feinberg Graduate School of The Weizmann Institute of Science, **1993**.
[21] G. Abrahamsson, G. Larsson, E. von Sydow, *Acta Cryst.* **1960**, *13*, 770.
[22] J. D. Dunitz, *X-ray Analysis of the Structure of Molecules*; Cornell University Press, Ithaca, NY, **1979**; pp. 43–49.
[23] Fitting of the Bragg rod data in these structures was found to be rather insensitive to variations in the atomic displacement parameter u_z along the normal to the water surface. In keeping with GID analysis of amphiphilic molecules $C_{20}H_{39}CO_2H$, and $C_{19}H_{39}CO_2C_nH_{2n}OH$ ($n = 9, 10$), u_z is 0.5–1.0 $Å^2$.
[24] M. C. Shih, T. M. Bohanon, J. M. Mikrut, P. Zschack, P. Dutta, *Phys. Rev. A* **1992**, *45*, 5734.
[25] a) D. W. Peterson, H. A. Levy, *Acta Cryst.* **1957**, *10*, 70; K. Shimaoko, *J. Phys. Soc. Jpn* **1960**, *15*, 106. b) K. J. Tauer, W. N. Lipscomb, *Acta Cryst.* **1952**, *5*, 606.
[26] K. P. Bell, S. A. Rice, *J. Chem. Phys.* **1993**, *99*, 4160.
[27] J. Gao, W. L. Jorgensen, *J. Phys. Chem.* **1988**, *92*, 5813
[28] Q. Du, R. Superfine, E. Freysz, Y. R. Shen, *Phys. Rev. Lett.* **1993**, *70*, 2313.
[29] S. P. Weinbach, K. Kjaer, J. Als-Nielsen, M. Lahav, L. Leiserowitz, *J. Phys. Chem.* **1993**, *97*, 5200.